Pure appl. geophys. 166 (2009) 1649–1667
0033–4553/09/101649–19
DOI 10.1007/s00024-009-0515-0

Pure and Applied Geophysics

Geometry of the Nojima Fault at Nojima-Hirabayashi, Japan – I. A Simple Damage Structure Inferred from Borehole Core Permeability

David A. Lockner,[1] Hidemi Tanaka,[2] Hisao Ito,[3] Ryuji Ikeda,[4] Kentaro Omura,[5] and Hisanobu Naka[6]

Abstract—The 1995 Kobe (Hyogo-ken Nanbu) earthquake, M = 7.2, ruptured the Nojima fault in southwest Japan. We have studied core samples taken from two scientific drillholes that crossed the fault zone SW of the epicentral region on Awaji Island. The shallower hole, drilled by the Geological Survey of Japan (GSJ), was started 75 m to the SE of the surface trace of the Nojima fault and crossed the fault at a depth of 624 m. A deeper hole, drilled by the National Research Institute for Earth Science and Disaster Prevention (NIED) was started 302 m to the SE of the fault and crossed fault strands below a depth of 1140 m. We have measured strength and matrix permeability of core samples taken from these two drillholes. We find a strong correlation between permeability and proximity to the fault zone shear axes. The half-width of the high permeability zone (approximately 15 to 25 m) is in good agreement with the fault zone width inferred from trapped seismic wave analysis and other evidence. The fault zone core or shear axis contains clays with permeabilities of approximately 0.1 to 1 microdarcy at 50 MPa effective confining pressure (10 to 30 microdarcy at *in situ* pressures). Within a few meters of the fault zone core, the rock is highly fractured but has sustained little net shear. Matrix permeability of this zone is approximately 30 to 60 microdarcy at 50 MPa effective confining pressure (300 to 1000 microdarcy at *in situ* pressures). Outside this damage zone, matrix permeability drops below 0.01 microdarcy. The clay-rich core material has the lowest strength with a coefficient of friction of approximately 0.55. Shear strength increases with distance from the shear axis. These permeability and strength observations reveal a simple fault zone structure with a relatively weak fine-grained core surrounded by a damage zone of fractured rock. In this case, the damage zone will act as a high-permeability conduit for vertical and horizontal flow in the plane of the fault. The fine-grained core region, however, will impede fluid flow across the fault.

Key words: Nojima fault, fault structure, permeability, strength, Kobe earthquake.

[1] US Geological Survey, 345 Middlefield Rd MS977, Menlo Park, CA 94025, USA.
E-mail: dlockner@usgs.gov

[2] Department of Earth and Planetary Sciences, University of Tokyo, Tokyo, Japan.

[3] Center for Deep Earth Exploration, Japan Agency for Marine-Earth Science and Technology, Yokohama, Japan.

[4] Department of Earth and Planetary Sciences, Hokkaido University, Hokkaido, Japan.

[5] National Research Institute for Earth Science and Disaster Prevention, Tsukuba, Japan.

[6] Ehime University, Matsuyama, Japan.

1. Introduction

The scientific drillholes crossing the Nojima fault at depth in the epicentral region of the 1995 Kobe earthquake, M = 7.2, provide a unique opportunity to study the mechanical and fluid transport properties of an active fault immediately after a major rupture event. Most first-hand evidence of the properties of active faults comes from examination of surface exposures that have typically undergone long and complicated histories of uplift and alteration. Examination of fault rock associated with rupture nucleation or significant energy release on strike-slip faults presents a particular problem since there is little vertical slip to bring deeper rocks to the surface. Seismic, gravity, electromagnetic and other remote sensing techniques can provide information about the deep structure of active faults, however a complete understanding of fault zone properties in the hypocentral regions of damaging earthquakes requires direct observation by the drilling of deep scientific boreholes. Recent examples of these include the boreholes crossing the Nojima fault, the Taiwan Continental Drilling Program TCDP (crossing at 1.1 km depth the Chelungpu fault that slipped in the 1999 Chi-Chi earthquake) (Ma *et al.*, 2006) and the San Andreas Fault Observatory at Depth SAFOD (crossing at 3 km depth the San Andreas fault near Parkfield, California (Hickman *et al.*, 2004).

Some recent studies of exhumed fault zones, especially mature zones that have sustained large total offset (Faulkner *et al.*, 2003; Wibberley and Shimamoto 2003) reveal broad, complex structures with multiple slip surfaces and highly variable permeability. Logging data of the SAFOD borehole show a similar complex structure with at least two active strands separated by broad zones of material with fluctuations in seismic velocity, resistivity and density (Hickman *et al.*, 2007). While the active traces of the San Andreas at SAFOD are centimeters in width, they are embedded in zones of heterogeneous material that has undergone shearing, rotation and mixing over the history of the fault.

At the other end of the spectrum of fault zone complexity are numerous laboratory and field observations of much simpler fault zone structures. Probably the simplest form, as suggested by studies of exhumed faults (Caine *et al.*, 1996; Caine and Forster, 1999; Chester *et al.*, 1993; Chester and Logan, 1986), consists of a narrow clay-rich or fine-grained core surrounded by a damage zone of highly fractured rock. The bulk of the shear deformation associated with the fault occurs in the narrow core zone, implying that this is the weakest portion of the fault structure. However, due to the fine grain size of the clay or crushed material in the fault core, it is expected to have a relatively low permeability. In addition to mesoscopic fractures, the surrounding damage zone contains a high density of microcracks, both within and between grains, although it is likely to have sustained relatively little total shear strain. Similar structures have been observed in laboratory samples that have been loaded to failure in shear (Moore and Lockner, 1995). If the fault occurs in low-porosity crystalline rock (such as the granodiorite of the Nojima fault), the high crack density in the damage zone results in significant pore volume increase and an increase in transport properties such as fluid permeability (Caine *et al.*, 1996; Caine and

Forster, 1999) and electrical conductivity (Lockner and Byerlee, 1986). Furthermore, the fact that shear has been captured repeatedly by the narrow fault core implies that this material should have lower strength than the surrounding host rock and damage zone material. The contrast in material properties between damage zones associated with active faults and the surrounding country rock can often be observed at macroscopic to near crustal scales with remote geophysical techniques such as magnetotelluric and seismic profiling. Most recently, trapped seismic waves, in which the fault zone acts as a waveguide, have been observed in active faults (Ben-Zion *et al.*, 2003; Li and Leary, 1990), and in particular on the Nojima fault (Li *et al.*, 1998).

The M7.2 Kobe earthquake nucleated beneath the Akashi Strait on January 17, 1995 (Fig. 1). The surface rupture on Awaji Island (to the SW of the epicenter) was about 10 km in length with 1 to 2 meters of lateral offset along the Nojima fault (Lin *et al.*, 1995; Lin and Uda, 1996; Nakata *et al.*, 1995). Surface rupture progressively diminished for about 13 km to the SW of the epicenter (Lin and Uda, 1996). Two scientific drillholes, crossing the Nojima fault 7 km SW of the epicenter at Nojima-Hirabayashi, were initiated about one year after the earthquake by the Geological Survey of Japan (GSJ) and the National Research Institute for Earth Science and Disaster Prevention (NIED). The GSJ borehole site was 75 m to the SE of the fault trace and crossed the fault at an oblique angle at a depth of 624 meters (Fig. 2). Fault core material at this depth contained smectite and other weak clay but also significant amounts of fine-grained quartz, feldspar, calcite and relatively strong alteration minerals (Mizoguchi *et al.*, 2008; Moore *et al.*, 2008; Ohtani *et al.*, 2000; Tanaka *et al.*, 2001, 2007). The NIED hole was started 302 m to the SE of the fault trace. This drillhole intersected two clay-rich shear zones at depths of 1140 m and 1312 m. A more diffuse shear zone was also crossed at about 1800 meters (see Fig. 2). These three zones are referred to in this paper as the 1140, 1312, and 1800 m NIED shear zones. Strength and permeability measurements reported here, as well as petrographic observations presented by (Moore *et al.*, 2008), all indicate that unlike the other shear zone crossings, the 1800 m NIED shear zone was not activated by the 1995 Kobe earthquake. Tanaka *et al.* (2007) concluded that the main slip of the Kobe earthquake occurred at the 1140 m shear zone. In their interpretation, based on petrographic analysis, geochemistry and well-logging data, the Nojima Fault Zone (NFZ) spanned a minimum depth range in the NIED borehole from 1054.0 to 1189.6 m (Fig. 2).

In the present study, we report on laboratory tests of 22 core samples taken from the NIED and GSJ drillholes following the Kobe earthquake. Rock strength and matrix permeability measurements were carried out to provide fault zone properties for profiles across the fault at two depths. Due to the limited number of samples and the difficulties associated with sample preparation, this study was intended to be exploratory in nature. In fact, the permeability and strength measurements are in excellent agreement with the idealized fault structural model described above. Additional data regarding petrography and microcrack characteristics are provided in a companion paper (Moore *et al.*, 2008).

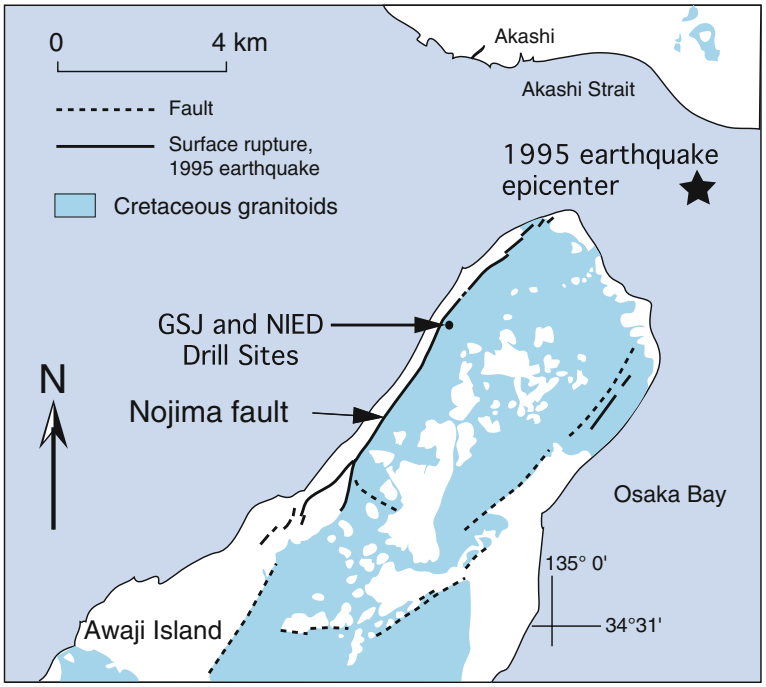

Figure 1
Map detailing 1995 Kobe earthquake epicenter (star) and surface rupture reported on Awaji Island. Rupture was on the Nojima fault following the NW shore of the island. GSJ and NIED drill sites were about 7 km from the epicenter near Nojima-Hirabayashi. The rupture also extended NE from the epicenter past Kobe (not shown on map).

2. *Experimental Technique*

Protolith rock for the Nojima fault in the vicinity of the boreholes is a biotite-hornblende granodiorite (OHTANI *et al.*, 2000; TANAKA *et al.*, 2001). A set of 22 samples was selected from the NIED and GSJ boreholes. Due to the limited number, sample selection was concentrated about the obvious shear zones in an attempt to obtain representative profiles across the fault zone structures. Depth intervals where samples were taken are indicated in Figure 2. Significant variability of rock type exists in the shear zones and a more complete evaluation of fault zone properties would require a much denser and more systematic sampling of the drill core than was possible in this study. Preferred sample dimensions were nominally 25.4 mm-diameter by 50.8 mm-length cylinders. Much of the recovered drill core (especially in the damage zones) had little or no cohesion and contained hard grain fragments. As a result, many samples were impossible to prepare to these preferred dimensions. If samples could not be prepared as cylinders an alternative shape in the form of rectangular prisms with 18.0 mm-square-cross section was attempted (Fig. 3). Most of the samples tested were of this type. These

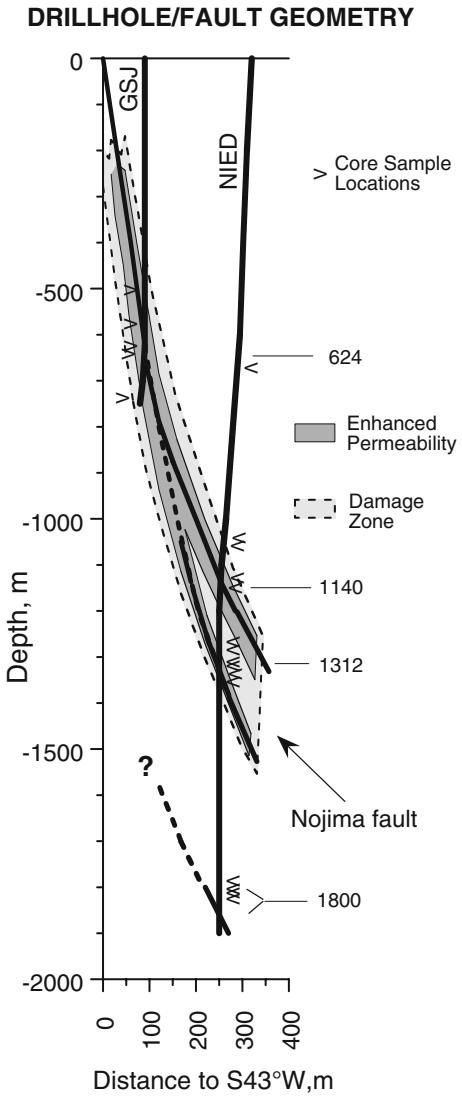

Figure 2

Schematic diagram of the Nojima fault (modified from TANAKA *et al.*, 2007) in the vicinity of the GSJ and NIED drillholes, showing the depths at which fault zones were intersected. The trend of the fault is N35E and, at the drill sites dips 84° to SE. A single fault trace was crossed by the GSJ drillhole while two activated strands were crossed by the NIED drillhole. A deeper fault zone was intersected at about 1800 m, but analysis of core samples indicates that this is a relic fault that was not reactivated by the 1995 Kobe earthquake. Sample depths tested in this study are indicated by '>'. A broad damage zone, shown in light gray, ($\sim$70 m wide) is inferred from microcracks and other petrographic evidence reported by TANAKA *et al.* (2007). The narrower damage envelopes (dark gray) indicate zones of enhanced permeability observed in this study (see Discussion).

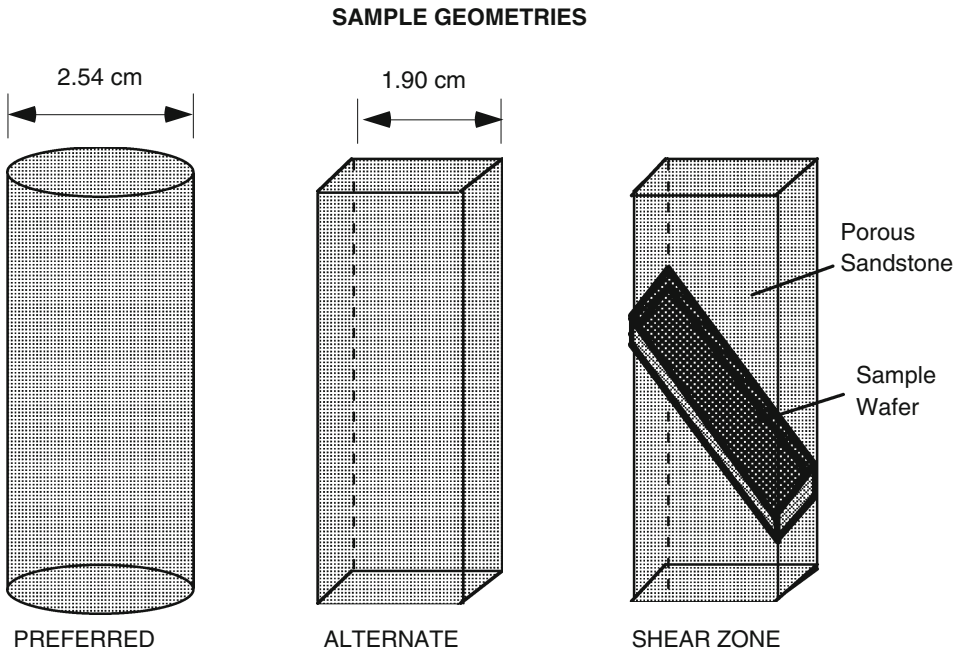

Figure 3
Diagram showing the three sample shapes used in this study. Whenever possible, right-cylinders were prepared. Most of the damage zone samples had little cohesion and could not be cored. In this case, rectangular prisms were cut from the drill core material. Only limited amounts of fault core material were available. We were able to cut wafers of this material (thicknesses of 1 to 2 cm) that were sheared between porous sandstone driving blocks with saw cut surfaces inclined by 30°.

intact samples were prepared so that their long axis was subparallel to the drill hole axis and therefore subvertical. The clay-rich shear zone core samples were available in limited quantities and sliced to provide wafers with a thickness in the 1 to 2 cm range. These were placed between porous sandstone driving blocks cut at an angle of 30° to the sample column axis.

Samples were jacketed and loaded in a standard triaxial deformation apparatus. Each sample was evacuated and then saturated with distilled, deionized water. Permeability was measured using a constant flow rate method at effective confining pressure of 10, 30, and 50 MPa. Test samples were oriented parallel to the original borehole cores so that the reported permeability and strength data are essentially for flow and maximum compressive stress in a subvertical orientation. No attempt was made to determine anisotropy in either permeability or strength. Following the hydrostatic permeability measurements, each sample was loaded incrementally at constant effective confining pressure of 50 MPa until failure occurred. Following each strain increment along the loading path, deformation was halted and permeability was determined as indicated in Figure 4. After peak stress, deformation continued to 5 mm axial shortening at a rate of 0.48 μm/sec with periodic pauses to repeat permeability measurements.

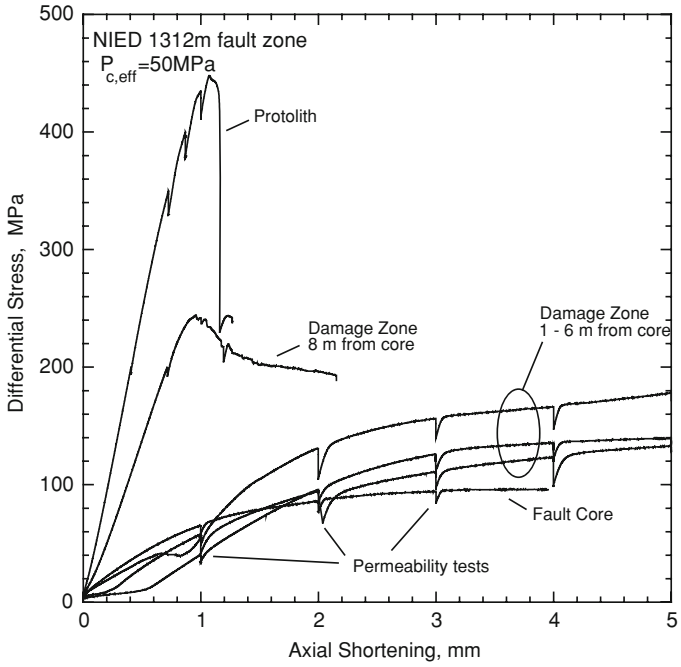

Figure 4

Differential stress plotted as a function of axial shortening for representative samples from NIED 1312 m fault zone. Periodic stress drops indicate times when deformation was stopped to measure permeability. The strongest sample is undamaged granodiorite protolith sampled outside the fault zone. The weakest sample is fault core material. Intermediate strength samples are taken from the damage zone within 8-m horizontal distance from the fault core. All deformation tests were run under drained conditions (saturated with deionized water) at constant confining pressure of 50 MPa and axial shortening rate of 0.48 μm/sec.

Accuracy of the permeability measurements is difficult to determine since some samples had less than ideal surface finishes and some permeabilities were near either the high or low limits of our measuring capabilities; sample permeabilities ranged from less than 1×10^{-9} to 3×10^{-3} Darcy (1 Darcy $= 10^{-12}$ m^2). The lower limit for our measuring system was 0.3 nDa. Absolute permeability uncertainties reported here are less than $\pm$ 25% while relative uncertainties in a single experiment are 5 to 10%.

3. Results

3.1. Rock Strength

Care was taken during sample preparation to preserve the intrinsic grain structure and cohesion to the extent possible. Obvious changes did occur in the samples due to drying and decompression of the original drill cores. However, these changes were minimized as

much as possible with the expectation that the *in situ* rock properties would be preserved to large extent. Thin section observation (Moore *et al.*, 2008) revealed that while damage zone samples contained large microcrack densities, the relative position of grains remained, for the most part, intact. Therefore, any additional damage sustained during core retrieval did not result in disaggregation and loss of material. In fact, percentage of core recovery was excellent. One way to evaluate the extent of microcrack damage is to look for trends in the peak strength data for the various samples. Samples were tested at 50 MPa effective confining pressure, which is equivalent to approximately 3 km burial depth (assuming hydrostatic pore pressure gradient and average rock density of 2.7 g/cm^3), to provide an easy means of comparing sample to sample strength. A suite of stress-displacement plots for the 1312 m NIED fault trace is plotted in Figure 4. Periodic drops in strength indicate the times when deformation was stopped to make permeability measurements. In all cases, resumption of deformation resulted in strength recovery back to the original loading curve. Also included for comparison is the strongest sample, taken from a depth of 659.3 meters, well above the fault and representing strength of the undamaged protolith. The weakest sample is clay-rich fault core material taken from 1312.0 meters. Four other lines plotted in Figure 4 show strengths of samples taken from the damage zone. The sample taken 8 meters (horizontal distance) from the fault core has sustained significant damage (strength is about half of the protolith strength) and passes through a peak in strength before dropping to residual frictional strength. The initial loading slope of this sample is less than the loading slope for the protolith material, indicating that damage has reduced the elastic modulus. Other damage zone samples taken closer to the fault core undergo strain hardening without passing through a peak in strength. These samples have sustained enough damage (either *in situ* or during sample retrieval) to eliminate most of their cohesive strength. In this case, final strength is frictional sliding strength and is correlated to the relative amount of clay and other weak alteration minerals within each sample.

Peak strength data for the four shear zone crossings in the GSJ and NIED boreholes are presented in Figure 5 as the ratio of shear to normal stress (μ) resolved on a plane inclined 30° to the sample axis. The actual inclination of the experimentally induced fracture plane was difficult to determine in many of the strength tests, and 30° provides a satisfactory approximation for comparison of different samples. Calculated this way, normalized strength for the intact granodiorite protolith is $\mu_{\text{intact}} = 1.18$. (Note that this value is greater than what is commonly referred to as coefficient of internal friction, defined as the tangent to the Mohr-Coulomb failure envelope.) Peak differential stress, σ_Δ, which is the quantity measured directly in the experiments, can be recovered from the data in Figure 5 by the formula $\sigma_\Delta = 200\mu/(1.732\text{-}\mu)$ (expressed in MPa).

The horizontal axis in Figure 5 is the horizontal distance between the center of the fault zone and the *in situ* location of each core sample. Given the fault/borehole geometry shown in Figure 2, this horizontal distance is 5 to 10 percent greater than the perpendicular distance to the fault surface. No distinct fault center could be identified for the 1800 m NIED fault zone thus the horizontal axis in Figure 5d could be shifted by a

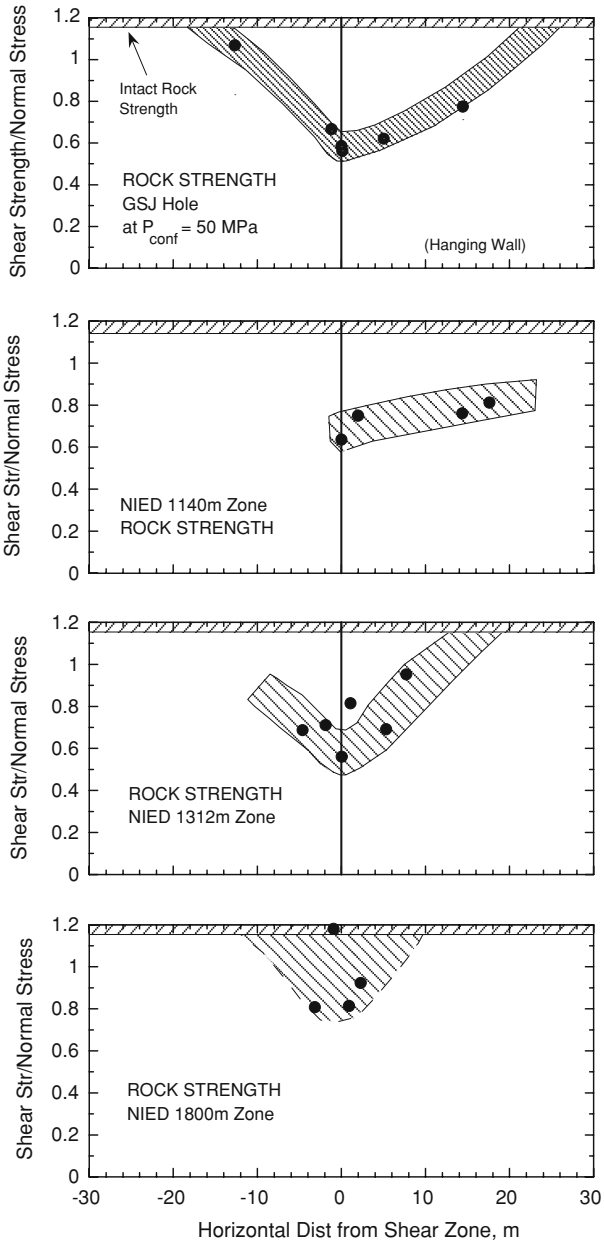

Figure 5

Profiles of peak shear strength divided by effective normal stress for the four fault zone crossings in the GSJ and NIED boreholes. Stresses are calculated for surfaces inclined 30° to maximum compressive stress direction (see text). Strength for the three active fault crossings is lowest in the fault zone core material and generally increases with distance from the core. One of the samples from the relic fault zone at 1800 m has strength similar to the protolith. The other thee deep samples have modest cohesive strength (peak strength is 5 to 20 percent higher than frictional sliding strength).

few meters. Notice that the three fault crossings with well-defined fault zone cores (Figs. 5a, 5b and 5c) all show a minimum in strength at the fault zone axis. This is consistent with the model described above in which nearly all displacement concentrates in the narrow fault core (a zone that is only a few centimeters wide in all three examples; TANAKA *et al.*, 2007). The general trend in these three examples is for strength to gradually increase with distance away from the fault zone axis. This gradual strength increase corresponds to a decrease in microcrack damage (*i.e.,* MOORE and LOCKNER, 1995; MOORE *et al.*, 2008). Damage zone half-width as suggested by the strength data in Figures 5a–5c is 15 to 25 m. While the fault core material was the weakest in all three examples, the minimum frictional sliding strength ($\mu \sim 0.55$) is significantly stronger than for smectite or other weak phyllosilicates (μ of 0.1 to 0.3) (MOORE and LOCKNER, 2004; 2007). TEMBE *et al.* (2008) have recently reported on frictional strength of quartz/smectite/illite mixtures where they found good correlation between strength of synthetic mixtures and strength of natural fault gouges. Frictional strength of 0.55 to 0.60 would imply, based on the TEMBE *et al.* (2008) analysis, a dry weight clay fraction of 20 to 35 percent for the Nojima fault core material. Thus, while weak clay minerals are present in the Nojima core samples, they apparently do not dominate the fault core composition.

The 1800 m NIED shear zone (Fig. 5d) is different from the other three examples. No distinct shear zone core was observed in the borehole samples. While the three shallower fault core zones showed strength significantly less than the protolith strength (μ in the range 0.55 to 0.62 as compared to protolith strength of 1.18), rock strength from the 1800 m zone is significantly greater ($\mu \sim 0.8$). Apparently this deep zone was not activated in the Kobe earthquake and has, over time, been restrengthening by vein filling and mineral alteration (MOORE *et al.*, 2008).

3.2. Rock Matrix Permeability

All permeability measurements are plotted as a function of axial stress in Figure 6. The first three measurements of each test at 10, 30, and 50 MPa were conducted without deviatoric stress and represent the permeability loss due to an increase in effective confining pressure. Permeability typically dropped by two to three orders of magnitude as microcracks closed in response to this hydrostatic loading. The remainder of each curve at axial stress above 50 MPa in Figure 6 represents the deformation tests at 50 MPa effective confining pressure. Initially, all samples showed loss of permeability with increasing deviatoric stress. By approximately 50% peak stress, the more competent samples began to exhibit increasing permeability with increasing deviatoric stress. This reversal from permeability decrease to permeability increase corresponds to the onset of dilatancy and the opening of microcracks within the sample (see, for example, ZOBACK and BYERLEE, 1975 and similar trends in electrical conductivity, LOCKNER and BYERLEE, 1986). The clay-rich fault core samples did not show dilatant behavior. Instead, they showed a steady loss of permeability with continued shearing and strain hardening. This behavior is similar to shear-enhanced compaction in porous sandstone as discussed by

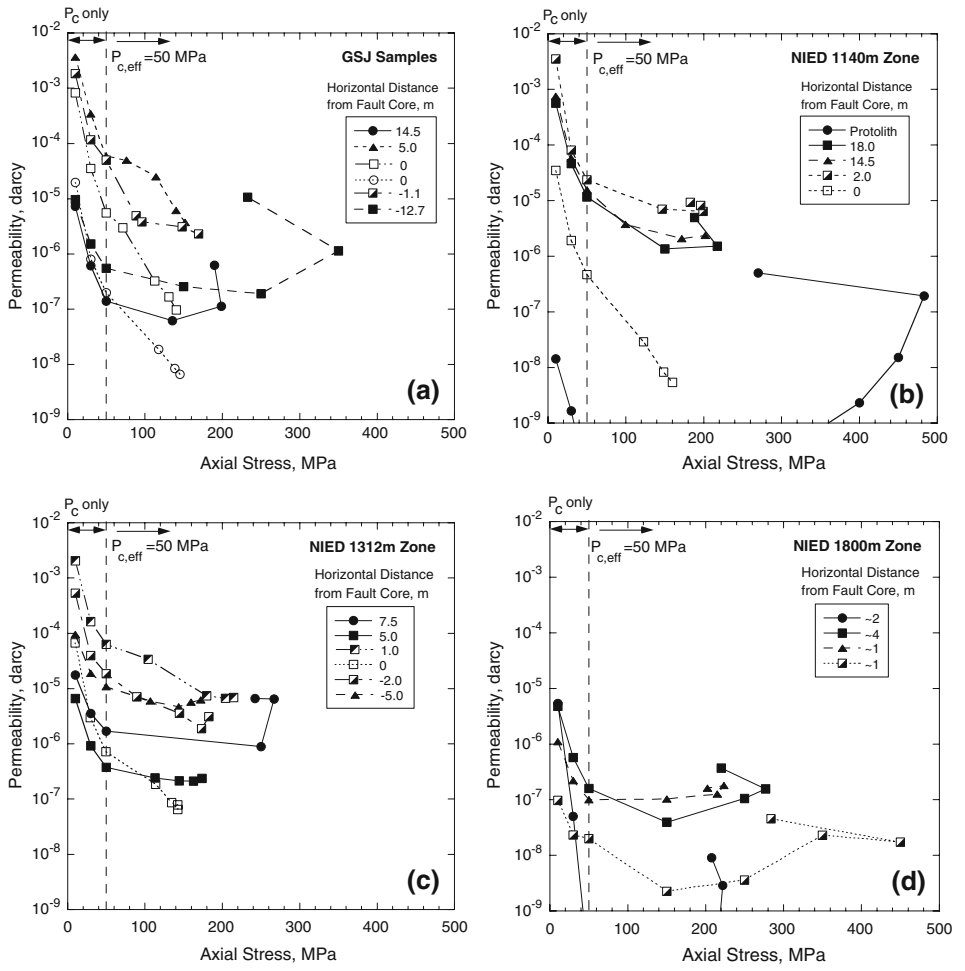

Figure 6

Permeability plotted versus axial load for GSJ and NIED samples. Pressurization to 50 MPa is hydrostatic loading without deviatoric stress. Permeability decreased by 2 to 3 orders of magnitude in response to application of 50 MPa confining pressure. Data for axial stress above 50 MPa show permeability change in response to sample deformation at 50 MPa effective confining pressure. All samples show an initial decrease in permeability with application of deviatoric stress. More competent samples sustained opening of microcracks at higher stresses and a corresponding increase in permeability. Some samples failed by forming through-going fractures. In these cases, plots show a drop in strength for the final permeability measurement that measured flow across the newly formed fault surface. Weaker samples (especially fault core samples) sustained continued grain crushing and compaction so that permeability steadily decreased with deformation.

Wong and Baud (1999). The protolith granodiorite shown as the low permeability curve, Figure 6b, is a dense crystalline rock with low matrix permeability. In this case, application of deviatoric stress reduced the permeability below the measurement limit of our test system. By 400 MPa axial load, however, new dilatant cracks had increased

Figure 7 ►

Profiles of matrix permeability measured at 50 MPa effective confining pressure. The three upper fault crossings show a low permeability fault core (fine-grained material containing some clay fraction) surrounded by high permeability damage zones (interlocked grains with numerous open microfractures). The deep shear zone is partially sealed and was apparently not activated by the Kobe earthquake.

permeability to a measurable level, which continued to increase to peak axial load of 483 MPa. Another trend observable in Figure 6 is a systematic decrease in peak strength of samples from the intact protolith, through the damage zone samples to the fault core samples. The low strength of the fault core is consistent with the concentration of shear deformation in this zone.

We have already noted that the permeability of all samples shows a strong sensitivity to increases in effective confining pressure. All of the examples plotted in Figure 6 show a decrease of two to three orders of magnitude for a 50 MPa pressure increase. This pressure sensitivity is indicative of rocks in which flow is through low aspect ratio cracks (long, thin microcracks) that can open or close flow paths in response to small pressure changes (MORROW *et al.*, 1994). This type of microcrack is more susceptible to changes in permeability resulting from vein filling than the more equant pores that might be found, for example, in a porous sandstone.

Because of the strong pressure sensitivity of permeability in these samples, we expect that *in situ* permeability in the Nojima fault zone will decrease rapidly with depth. For example, the GSJ samples, with a fault crossing depth of 624 m would have an effective overburden pressure of approximately 11 MPa while the 1312 m NIED crossing overburden pressure would be about 22 MPa. The maxima in the damage zone permeabilities adjusted for these effective pressures would then be 3.3 mDa and 0.45 mDa, respectively.

To provide a more direct comparison of the different fault zone permeability measurements, we have plotted matrix permeability profiles in Figure 7 using experimental values from 50 MPa effective confining pressure, equivalent to 3 km burial depth. *In situ* permeabilities for the GSJ hole (at 11 MPa) would be about 50 times larger than the values shown in Figure 7. As with the strength data, the three shallow crossings show permeability profiles similar to the idealized fault zone model described above. The fault zone axis, due to its clay content and fine gouge grain size, has relatively low permeability in the microdarcy range. Flanking the fault zone axis, the highly fractured damage zone has permeabilities in the 50 to 100 microdarcy range. Distantly from the fault zone axis, grain damage and permeability decrease until permeability returns to the protolith permeability value. The NIED borehole deep shear zone has permeability that is greater than the protolith permeability but significantly less than the shallower shear zone values. Thus both strength and permeability data suggest that the deep fault zone was not activated in the Kobe earthquake and is undergoing sealing and restrengthening.

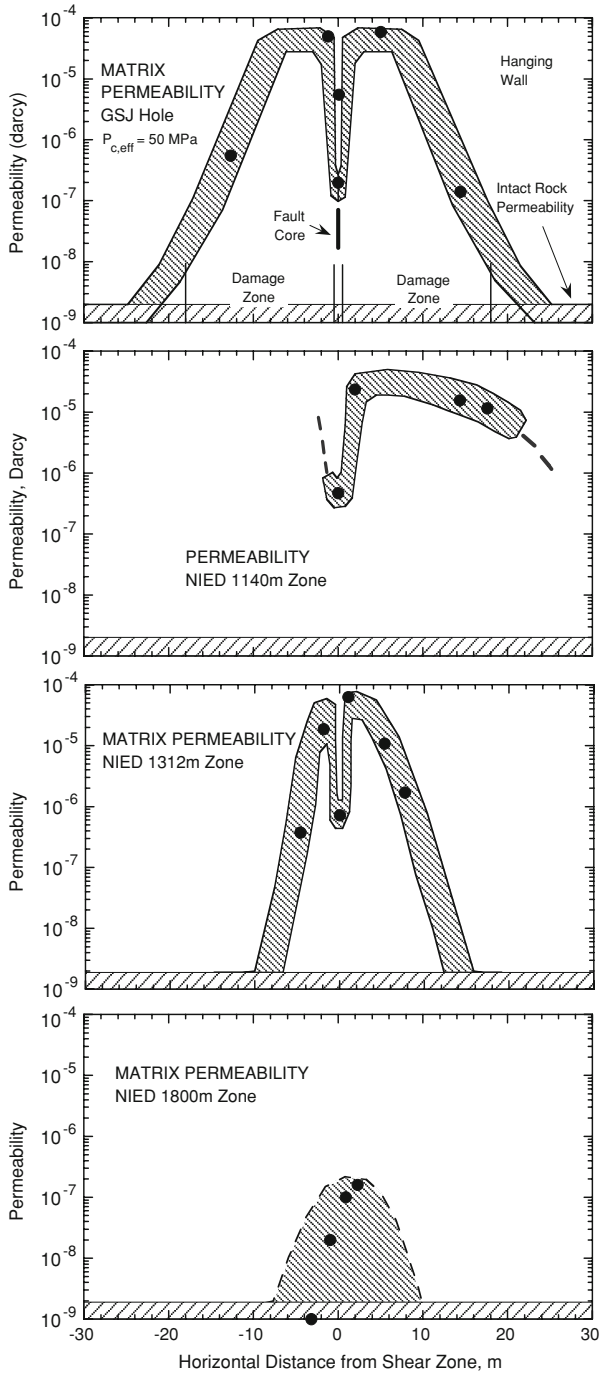
MATRIX
PERMEABILITY
GSJ Hole
$P_{c,eff}$ = 50 MPa
Hanging
Wall
Intact Rock
Permeability
Fault
Core
Damage
Zone
Damage
Zone
Permeability (darcy)
PERMEABILITY
NIED 1140m Zone
Permeability, Darcy
MATRIX PERMEABILITY
NIED 1312m Zone
Permeability
MATRIX PERMEABILITY
NIED 1800m Zone
Permeability
10^{-4}
10^{-5}
10^{-6}
10^{-7}
10^{-8}
10^{-9}
-30
-20
-10
0
10
20
30
Horizontal Distance from Shear Zone, m

4. Discussion

Our measurements of core sample strength and permeability are in good agreement with the idealized fault zone model described, for example, by Caine *et al.* (1996); Chester and Logan (1986) and Evans *et al.* (1997). We observe a thin, low-strength, low-permeability fault zone core flanked by zones of high permeability rock that have undergone relatively limited total shear. These observations imply that to depths of as much as 3 to 5 km, the postseismic fault zone will act as a high permeability fluid conduit for fluid flow in the plane of the fault. Because the fault core has low permeability it is likely to act as a barrier to fluid flow across the fault. However, this barrier is notably thin and may have a complex structure. For example, the Nojima fault zone appears to have branched into two shear zones between the GSJ and NIED borehole crossings. To the degree that this thin shear zone core is spatially discontinuous and anastomosed, its ability to act as a fluid barrier will be diminished. It is difficult to determine this three-dimensional structure at depth from a limited number of (typically one or two) borehole crossings.

Tanaka *et al.* (2007) concluded that the principal slip surface for the Kobe earthquake was crossed at 1140 m in the NIED borehole. Since we find reduced strength and enhanced permeability for both the 1140 and 1312 zones, it is likely that both of these fault segments were activated in the Kobe earthquake. In this case, the 1140 and 1312 zones could represent bounding faults of a fault zone that is about 130 m wide. Unfortunately, we did not sample the intervening depth interval in this reconnaissance study to determine transport or mechanical properties. Figure 2 has been modified from the original version in Tanaka *et al.* (2007) to highlight the possible damage zone surrounding the principal slip surfaces. Our measurements do suggest a more concentrated high-permeability zone associated with each slip surface embedded in a broader damage zone as suggested by the petrographic analysis of Tanaka *et al.* (2001, 2007). The damage zone half-width, as indicated by the permeability profiles ranges from 10 to 25 m. Based on trapped seismic wave analysis, Li *et al.* (1998) found a half width of approximately 15 m for the Nojima fault. Thus, direct measurements of both the permeability and strength of the fault zone indicate a damage zone half width that is consistent with the deeper seismic observations. Indeed, a similar geometry has been observed for the San Andreas Fault near Parkfield, California. The SAFOD drillhole encountered a broad damage zone containing two actively creeping strands (one of which appears to be more active) less than 100 m apart (Hickman *et al.*, 2005).

The permeability data shown in Figure 7 are all measured at 50 MPa effective confining pressure to allow for a more direct sample-to-sample comparison. All samples showed a strong sensitivity of permeability to confining pressure. Pressure sensitivity can be approximated by an exponential relation of the form

$$k = k_0 \exp\left(-P_{c,eff}/P^*\right), \tag{1}$$

where k_0 is permeability at zero pressure and P^* is a constant (see, for example, Rice, 1992). Permeability data plotted in Figure 6 at 10, 30 and 50 MPa effective pressure were

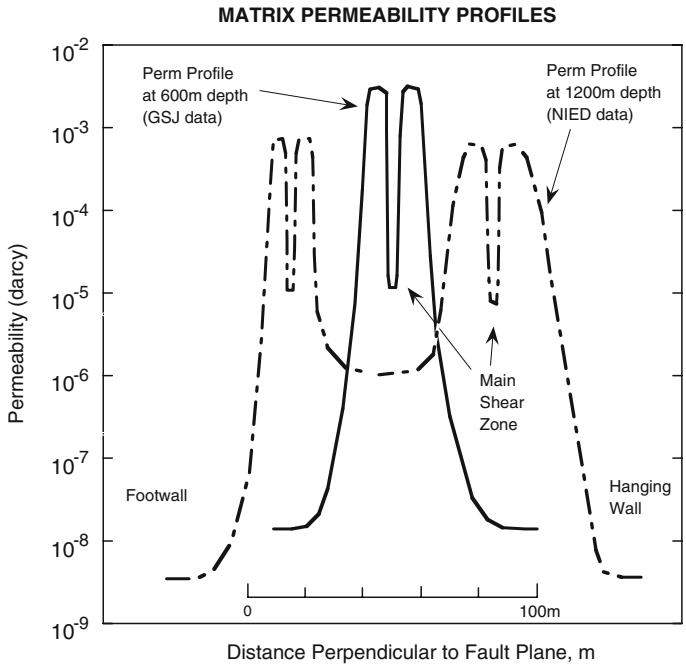

Figure 8
Interpretive profiles of permeability for Nojima fault at 600 and 1200 m depth. Permeabilities from data shown in Figure 6 have been adjusted for overburden stress using eq. (1). Additional information regarding damage zone width comes from TANAKA *et al.* (2007). Data from 1140 shear zone (Fig. 7b) and 1312 shear zone (Fig. 7c) have been combined to form the 1200 m profile. Distance is measured perpendicular to the fault plane (22° dip).

fit to (1) for each sample. All P^* values were similar and can be summarized by $P^* = 10.5 \pm 2.4$ MPa. Figure 8 shows two interpretive profiles of matrix permeability of the Nojima fault at Nojima-Hirabayashi. These profiles show permeability at depths of 600 and 1200 m for distance perpendicular to the fault plane. Effective confining pressure data from Figure 6 have been used with eq. (1) to adjust permeability for overburden pressure (assuming 2.7 g/cc average density and a hydrostatic pore pressure gradient). Additional evidence of the extent of the fault zone has come from TANAKA *et al.* (2007). The minimum in permeability at 1200 m depth between the two shear zones is not well constrained. Matrix permeability of the protolith is very low. For tight crystalline rock, bulk mesoscale permeability measured in the field is typically 1 to 2 orders of magnitude higher than matrix permeability due to dominance of fluid flow in fracture networks (BRACE, 1980).

Surface offset for the Kobe earthquake in this region was restricted to a single fault trace. This simple geometry extends to at least 600 m depth. Yet by 1200 m, the fault zone appears to have doubled in total width and developed a secondary splay fault. Still,

active slip surfaces are less than 1 meter in width, while the zones of intense damage, inferred from enhanced permeability, are 20 to 30 m wide and probably remain localized within the broader damage zone. Enhanced post-earthquake permeability in the damage zone is approximately 2 orders of magnitude greater that permeability of the fault core. Due to the tight crystalline protolith that hosts the Nojima fault in this region, fault core permeability is about 3 orders of magnitude greater than protolith matrix permeability and probably 1 to 2 orders of magnitude greater than protolith fracture-dominated bulk permeability.

The observations reported here provide a unique opportunity to understand fault zone properties at depth following a damaging earthquake. While we do not know the mechanical and hydraulic properties of the Nojima fault before the Kobe earthquake, it is likely that the violent rupture of the fault led to a sudden increase in permeability. This is consistent with observations following the 1989 Loma Prieta earthquake that enhanced fluid flow occurred in the epicentral region (Rojstaczer and Wolf, 1992). One important question not addressed by this study is how rapidly the enhanced fault zone permeability structure will be reduced by sealing and crack healing processes. The observation of increased strength and decreased permeability in the deep NIED fault zone indicates that these processes can significantly influence fault zone mechanics over the lifetime of an active fault. If this sealing and restrengthening process can occur over a single earthquake cycle as suggested by Sibson (1990; 1992), it could importantly influence repeat time, coseismic stress drop and rupture nucleation process. These thermally activated healing processes are expected to occur more quickly deeper in the fault zone where temperatures are higher. Laboratory observations (Moore *et al.*, 1994; 2001) indicate rapid and temperature-sensitive loss of matrix permeability in crystalline rocks under hydrothermal conditions. Observations of repeated sealing/opening cycles in thin sections taken from borehole samples (Moore *et al.*, 2008; Tanaka *et al.*, 2007) provide direct evidence that this process is operative in the Nojima fault. Observations of postseismic velocity recovery over periods of months to years (Li *et al.*, 2006; Peng and Ben-Zion, 2006) imply similar rapid changes in damage zone permeability and resistivity.

Development of off-fault damage during earthquakes is a topic of active research (Dor *et al.*, 2006). Recent studies suggest that asymmetry in off-fault damage should result from dynamic rupture propagation, either due to a contrast in material properties across the fault or the asymmetry in the dynamic stress field that propagates along the fault with the rupture front. In this study, off fault damage extending 15 to 25 meters from the fault core is clearly observed. While our core sampling is relatively sparse, we find little evidence for asymmetry in the damage zone structure as reflected by matrix permeability measurements. Since the GSJ and NIED boreholes are to the SW of the epicenter for a right-lateral fault, the tensile lobe of the dynamic stress field should be on the NW or footwall side of the fault (left-hand side of plots in Fig. 7). Figures 7a and 7c show no indication of enhanced damage on the footwall (left) side of the fault core. It is possible that the Nojima-Hirabayashi site is too near the epicenter of the earthquake for a

fully developed dynamic stress wave to have occurred. Or, the significant reverse faulting stress component may inhibit development of excessive damage in the footwall.

5. Conclusions

Laboratory measurements of matrix permeability and strength of core samples recovered from scientific drillholes at Nojima-Hirabayashi provide direct evidence for the structure of the fault damage zone and fault core associated with the Kobe earthquake. Numerous factors contribute to making the Nojima fault an ideal location for this type of analysis. The host rock is a competent, low-permeability, crystalline granodiorite that provides a clear contrast in strength and permeability to the fault zone properties. The fault zone architecture is relatively simple and easy to interpret. Also, surface rupture provides valuable constraints on magnitude and orientation of subsurface slip. At depths to 600 meters, the Nojima fault has a classic structure consisting of a narrow core of clay-rich fine-grained gouge surrounded by a zone of highly damaged rock. By 1200 m, the fault zone has broadened and may be bounded by the main shear zone (crossed at 1140 m) and a second branch (1312 m). Enhanced permeability is restricted to narrow zones around the active slip surfaces. Triaxial deformation tests show that the fault core material that captured most of the coseismic slip has the lowest strength. Damage zone samples have high microcrack densities and low cohesive strength and tend to be weaker close to the fault core. Matrix permeability provides an excellent method for differentiating the internal structure of the fault zone. The fine grain size of the fault core results in a reduced permeability of this material relative to the damage zone rock. While the fault core does contain clay, it has a relatively high shear strength ($\mu \sim 0.55$) indicating that the fault strength is still dominated by the unaltered quartz and feldspar constituents of the host rock as well as higher-strength carbonate precipitates. This study demonstrates the importance of obtaining fresh material from depth in active fault zones to unravel the structure and fault mechanics of these systems.

Acknowledgements

We thank J. Caine and C. Morrow and an anonymous reviewer for their helpful comments as well as useful discussions with the editors.

References

Ben-Zion, Y., Peng, Z., Okaya, D., Seeber, L., Armbruster, L.G., Ozer, N., Michael, A.J., Baris, S., and Aktar, M. (2003), *A shallow fault zone structure illuminated by trapped waves in the Karadere-Duzce branch of the North Anatolian Fault, western Turkey*, Geophys. J. Int., *152*, doi:10.1046/j.1365-246X.2003.01870.x, 699-717.

Brace, W. F. (1980), *Permeability of crystalline and argillaceous rocks*, Int. J. Rock Mech. Min. Sci. Geomech. Abstr. *17,* 241–251.

Caine, J.S., Evans, J.P., and Forster, C.B. (1996), *Fault zone architecture and permeability structure*, Geology *24*, 1025–1028.

Caine, J.S. and Forster, C.B., *Fault zone architecture and fluid flow: Insights from field data and numerical modeling*. In *Faults and Subsurface Flow in the Shallow Crust: AGU Geophysical Monograph, Vol. 113* (ed. Haneberg, W.C., Mozley, P.S., Moore, J.C. and Goodwin, L.B.) (Amer. Geophys. Union, Washington, D.C 1999), pp. 101-127.

Chester, F.M., Evans, J.P., and Biegel, R.L. (1993), *Internal structure and weakening mechanisms of the San Andreas fault*, J. Geophys. Res. *98*, 771–786.

Chester, F.M. and Logan, J.M. (1986), *Implications for mechanical properties of brittle faults from observations of the Punchbowl fault zone, California*, Pure Appl. Geophys. *124*, 79–106.

Dor, O., Ben-Zion, Y., Rockwell, T.K., and Brune, J. (2006), *Pulverized rocks in the Mojave section of the San Andreas fault zone*, Earth Planet. Sci. Lett. *245*, 642–654.

Evans, J.P., Forster, C.B., and Goddard, J.V. (1997), *Permeability of fault-related rocks, and implications for hydraulic structure of fault zones*, J. Structural Geol. *19*, 1393–1404.

Faulkner, D.R., Lewis, A.C., and Rutter, E.H. (2003), *On the internal structure and mechanics of large strike-slip fault zones: field observations of the Carboneras fault in southeastern Spain*, Tectonophysics *367*, 235–251.

Hickman, S., Zoback, M., Ellsworth, W., Boness, N., Malin, P., Roecker, S. and Thurber, C. (2007), *Structure and properties of the San Andreas Fault in central California: Recent results from the SAFOD experiment*, Scientific Drilling, Special Issue 1, 29–31.

Hickman, S.H., Zoback, M.D., and Ellsworth, W.E. (2004), *Introduction to special section: Preparing for the San Andreas Fault Observatory at Depth*, Geophys. Res. Lett. *31*, L12S01.

Hickman, S.H., Zoback, M.D., and Ellsworth, W.E. (2005), *Structure and composition of the San Andreas fault zone at Parkfield: Initial results from SAFOD Phases 1 and 2*, EOS Trans. AGU, *86*(52), Fall Meeting Suppl., Abstract T23E-05.

Li, Y.-G., Aki, K., Vidale, J.E., and Alvarez, M.G. (1998), *A delineation of the Nojima fault ruptured in the M7.2 Kobe, Japan, earthquake of 1995 using fault zone trapped waves*, J. Geophys. Res. *103*, 7247–7263.

Li, Y.-G., Chen, P., Cochran, E.S., Vidale, J.E., and Burdette, T. (2006), *Seismic evidence for rock damage and healing on the San Andreas Fault associated with the 2004 M 6.0 Parkfield earthquake*, Bull. Seismol. Soc. Amer. *96, doi:*10.1785/0120050803, S349-S363.

Li, Y.-G. and Leary, P. (1990), *Fault zone seismic trapped waves*, Bull. Seismol. Soc. Am. *80*, 1245–1271.

Lin, A., Imiya, H., Uda, S., Iinuma, K., Misawa, T., Yoshida, T., Abematsu, Y., Wada, T., and Kawai, K. (1995), *Investigation of the Nojima earthquake fault occurred on Awaji Island in the southern Hyogo prefecture earthquake (in Japanese with English abstract)*, J. Geogr. *104*, 113–126.

Lin, A. and Uda, K. (1996), *Morphological characteristics of the earthquake surface ruptures on Awaji Island, associated with the 1995 southern Hyogo Prefecture earthquake*, Isl. Arc *5*, 1–15.

Lockner, D.A. and Byerlee, J.D. (1986), *Changes in complex resistivity during creep in granite*, Pure Appl. Geophys. *124*, 659–676.

Ma, K.-F., Tanaka, H., Song, S.-R., Wang, C.-Y., Hung, J.-H., Tsai, Y.-B., Mori, J., Song, Y.-F., Yeh, E.-C., Soh, W., Sone, H., Kuo, L.-W., and Wu, H.-Y. (2006), *Slip zone and energetics of a large earthquake from the Taiwan Chelungpu fault Drilling Project*, Nature *444*, 473–476.

Mizoguchi, K., Hirose, T., Shimamoto, T., and Fukuyama, E. (2008), *Internal structure and permeability of the Nojima fault, southwest Japan*, J. Struct. Geol. *30*, 513–524.

Moore, D.E. and Lockner, D.A. (1995), *The role of microcracking in shear-fracture propagation in granite*, J. Struct. Geol. *17*, 95–114.

Moore, D.E. and Lockner, D.A. (2004), *Crystallographic controls on the frictional behavior of dry and water-saturated sheet-structure minerals*, J. Geophys. Res. *109*, doi:10.1029/2003JB002582.

Moore, D.E. and Lockner, D.A., *Friction of the smectite clay montmorillonite: A review and interpretation of data*. In *The Seismogenic Zone of Subduction Thrust Faults, MARGINS Theoretical and Experimental Science Series* (eds. Dixon, T.H. and Moore, J.C.) (Columbia University Press, New York 2007), pp. 317–345.

Moore, D.E., Lockner, D.A., and Byerlee, J.D. (1994), *Reduction of permeability in granite at elevated temperatures*, Science *265*, 1558–1561.

MOORE, D.E., LOCKNER, D.A., ITO, H., IKEDA, R., TANAKA, H., and OMURA, K. (2008), *Geometry of the Nojima fault at Nojima-Hirabayashi, Japan - II. Microtructures and their implications for permeability and strength*, Pure Appl. Geophys., in press.

MORROW, C., LOCKNER, D.A., HICKMAN, S., RUSANOV, M., and RÖCKEL, T. (1994), *Effects of lithology and depth on the permeability of core samples from the Kola and KTB drill holes*, J. Geophys. Res. *99*, 7263-7274.

MORROW, C.A., MOORE, D.E., and LOCKNER, D.A. (2001), *Permeability reduction in granite under hydrothermal conditions*, J. Geophys. Res. *106*, 30,551–30,560.

NAKATA, T., YOMOGIDA, K., ODAKA, J., SAKAMOTO, T., ASAHI, K., and CHIDA, N. (1995), *Surface fault ruptures associated with the 1995 Hyogoken-Nabu earthquake (in Japanese with English abstract)*, J. Geogr. *104*, 127–142.

OHTANI, T., FUJIMOTO, K., ITO, H., TANAKA, H., TOMIDA, N., and HIGUCHI, T. (2000), *Fault rocks and past to recent fluid characteristics from the borehole survey of the Nojima fault ruptured in the 1995 Kobe earthquake, southwest Japan*, J. Geophys. Res *105*, 16,161–16,171.

PENG, Z. and BEN-ZION, Y. (2006), *Temporal changes of shallow seismic velocity around the Karadere-Duzce branch of the north Anatolian fault and strong ground motion*, Pure Appl. Geophys. *163,* doi:10.1007/s00024-005-0034-6, 567-600.

RICE, J.R., *Fault stress states, pore pressure distributions, and the weakness of the San Andreas fault*. In *Fault Mechanics and Transport Properties of Rocks* (eds. Evans, B. and Wong, T.-f.) (Academic Press, London 1992) pp. 475–503.

ROJSTACZER, S. and WOLF, S. (1992), *Permeability changes associated with large earthquakes: An example from Loma Prieta, California*, Geology, 211–214.

SIBSON, R. H. (1990), *Conditions for fault-valve behavior*. In *Deformation Mechanisms, Rheology and Tectonics* (eds. Knipe, R.J. and Rutter, E.H.) (Geol. Soc. Special Publ. 1990) pp. 15–28.

SIBSON, R.H. (1992), *Implications of fault-valve behavior for rupture nucleation and recurrence*, Tectonophys. *211*, 283–293.

TANAKA, H., FUJIMOTO, K., OHTANI, T., and ITO, H. (2001), *Structural and chemical characterization of shear zones in the freshly activated Nojima fault, Awaji Island, southwest Japan*, J. Geophys. Res. *106*, 8789–8810.

TANAKA, H., OMURA, K., MATSUDA, T., IKEDA, R., KOBAYASHI, K., MURAKAMI, M., and SHIMADA, K. (2007), *Architectural evolution of the Nojima fault and identification of the activated slip layer by Kobe earthquake*, J. Geophys. Res. *1123,* B07304, doi:10.1029/2005JB003977.

TEMBE, S., LOCKNER, D.A., and WONG, T.-f. (2008), *Effect of clay content and mineralogy on frictional sliding behavior of simulated gouges: Binary and ternary mixtures of quartz, illite and montmorillonite*, J. Geophys. Res., *submitted*.

WIBBERLEY, C.A.J. and SHIMAMOTO, T. (2003), *Internal structure and permeability of major strike-slip fault zones: The median tectonic line in Mie Prefecture, Southwest Japan*, J. Struct. Geol. *25*, 59–78.

WONG, T-f. and BAUD, P. (1999), *Mechanical compaction of porous sandstone*, Oil & Gas Sci. Tech. –Rev. IFP *54,* 715–727.

ZOBACK, M.D. and BYERLEE, J.D. (1975), *The effect of microcrack dilatancy on the permeability of Westerly granite*, J. Geophys. Res. *80*, 752–755.

(Received September 29, 2008, revised March 3, 2009)
Published Online First: June 27, 2009